Journal of Medicinal Chemistry

Article

Structure-guided Design of Highly Selective and Potent Covalent Inhibitors of ERK1/2

Richard A Ward, Nicola Colclough, Mairi Challinor, Judit Debreczeni, Key Eckersley, Gary Fairley, Lyman Feron, Vikki Flemington, Mark Andrew Graham, Ryan Greenwood, Philip Hopcroft, Tina D Howard, Michael James, Clifford D Jones, Christopher R Jones, Jonathan Renshaw, Karen Roberts, Lindsay Snow, Michael Tonge, and Kay Yeung

J. Med. Chem., **Just Accepted Manuscript** • DOI: 10.1021/acs.jmedchem.5b00466 • Publication Date (Web): 15 May 2015

Journal of Medicinal Chemistry is published by the American Chemical Society. 1155 Sixteenth Street N.W., Washington, DC 20036

Structure-guided Design of Highly Selective and Potent Covalent Inhibitors of ERK1/2

Richard A. Ward[a], Nicola Colclough, Mairi Challinor, Judit E. Debreczeni, Kay Eckersley, Gary Fairley, Lyman Feron, Vikki Flemington, Mark A. Graham, Ryan Greenwood, Philip Hopcroft, Tina D. Howard, Michael James, Clifford D. Jones, Christopher R. Jones, Jonathan Renshaw, Karen Roberts, Lindsay Snow, Michael Tonge and Kay Yeung.

Oncology & Discovery Sciences iMeds, AstraZeneca, Alderley Park, Macclesfield, SK10 4TG, UK.

[a] To whom correspondence should be addressed. Phone: +44 (0)1625 519045. E-mail: richard.a.ward@astrazeneca.com. Address: AstraZeneca, Mereside, Alderley Park, Macclesfield, Cheshire, SK10 4TG, United Kingdom.

Abstract

The RAS/RAF/MEK/ERK signaling pathway has been targeted with a number of small molecule inhibitors in oncology clinical development across multiple disease indications. Importantly, cell lines with acquired resistance to B-RAF and MEK inhibitors have been shown to maintain sensitivity to ERK1/2 inhibition by small molecule inhibitors. There are a number of selective, non-covalent, ERK1/2 inhibitors reported along with the promiscuous hypothemycin (and related analogues) which act via a covalent mechanism of action. This manuscript reports the identification of multiple series of highly selective covalent ERK1/2 inhibitors informed by structure-based drug design (SBDD). As a starting point for these covalent inhibitors, both reported ERK1/2 inhibitors and chemical series identified via high-throughput screening, were exploited. These approaches resulted in the identification of selective covalent tool compounds for potential *in vitro* and *in vivo* studies to assess the risks and or benefits of targeting this pathway through such a mechanism of action.

Abbreviations

ABT (1-aminobenzotriazole), GSH (glutathione), HTS (high throughput screening), PD (pharmacodynamic), PK (pharmacokinetics), LLE (ligand lipophilicity efficiency), LE (ligand efficiency), LC-MS (liquid chromatography–mass spectrometry), MOA (mechanism of action), SAR (structure-activity relationships), THP (tetrahydropyran).

Introduction

The RAS/RAF/MEK/ERK pathway plays a central role in controlling mammalian cell cycle progression, differentiation, protein synthesis, metabolism, survival, migration and senescence[1]. This pathway is regulated by a wide range of extracellular stimuli which result in activation of the RAS family of GTPases (KRAS, NRAS and HRAS), subsequently turning on the downstream

RAF protein kinases (B-RAF, c-RAF, and a-RAF). The main substrates of the RAF kinases are the MAPK/ERK kinases, MEK1, and MEK2, which then phosphorylate their only substrates, extracellular signal–regulated kinase ERK1 and ERK2[2]. ERK1 and ERK2 control the output of the RAS/RAF/MEK/ERK pathway by activating their many substrates, both nuclear and cytoplasmic[3,4], which include nuclear components, transcription factors, membrane proteins and protein kinases. Activation of the RAS/RAF/MEK/ERK signaling pathway results in extensive changes in gene expression mediated by phosphorylation of transcription factors which promote cell cycle progression and also regulate negative feedback mechanisms, for example by controlling the expression of dual-specificity phosphatases (DUSPs) can dephosphorylate and inactivate ERK1/2[5].

Constitutive activation of the RAS/RAF/MEK/ERK pathway through genetic alterations is associated with multiple human tumours. RAS genes are mutated in colorectal (50%), melanoma (20%) and pancreatic (90%) tumours, whereas mutations in b-RAF have been identified in melanoma (60%), thyroid (~50%) and colorectal (10%) tumours[6]. Due to the association of activation of the RAS/RAF/MEK/ERK pathway and the ongogenic phenotype, several small molecule inhibitors targeting b-RAF and MEK have been developed and entered clinical trials in multiple disease indications[7,8]. Data from clinical trials with the RAF inhibitors such as vemurafenib and dabrafenib demonstrate dramatic regression of melanomas carrying the BRAF V600E mutation[9], whereas BRAF wild-type tumours are refractory. However, acquired resistance to RAF inhibitors occurs in a significant subset of patients, primarily from genetic alteration resulting in RAS/RAF/MEK/ERK pathway reactivation[10-13]. Additionally, several selective and potent non-ATP-competitive allosteric MEK1/2 inhibitors have been developed and assessed in multiple clinical trials. Only limited efficacy as single agent therapies has been reported with MEK inhibitors, therefore combinations of MEK1/2 inhibitors and cytotoxic chemotherapy, and/or other targeted agents are being studied to expand the efficacy of this class of agents.

Direct targeting of ERK1/2, the key signaling node of the RAS/RAF/MEK/ERK pathway, provides another therapeutic option in tumours with mutations in RAS or b-RAF genes. ERK1/2 inhibition may also have clinical utility in overcoming acquired resistance to RAF and MEK inhibitors where RAS/RAF/MEK/ERK pathway reactivation has occurred. ERK1 and ERK2 are 85% identical by sequence (significantly higher in the ATP binding site) and share some, if not all, of their functions with reported inhibitors apparently active against both. A range of reversible ERK1/2 small molecule inhibitors have been disclosed (figure 1), including multiple examples in clinical development. These include MK8353/SCH900353 (likely related to SCH772984[14]), BVD-523[15] and GDC-0994[16], in addition to a selection of reported pre-clinical inhibitors[17-20]. Hypothemycin and analogues such as FR148083[21] have also been reported as irreversible covalent inhibitors of ERK1/2, targeting the residue Cys-166, which is located in the ATP pocket. Sequence analysis across the kinome suggests that 48 kinases share a cysteine in this position[22]. These reported inhibitors appear to be active across all of these kinases and therefore have limited utility in terms of assessing the benefits and risks associated with selectively targeting ERK1/2 via a covalent mechanism of action.

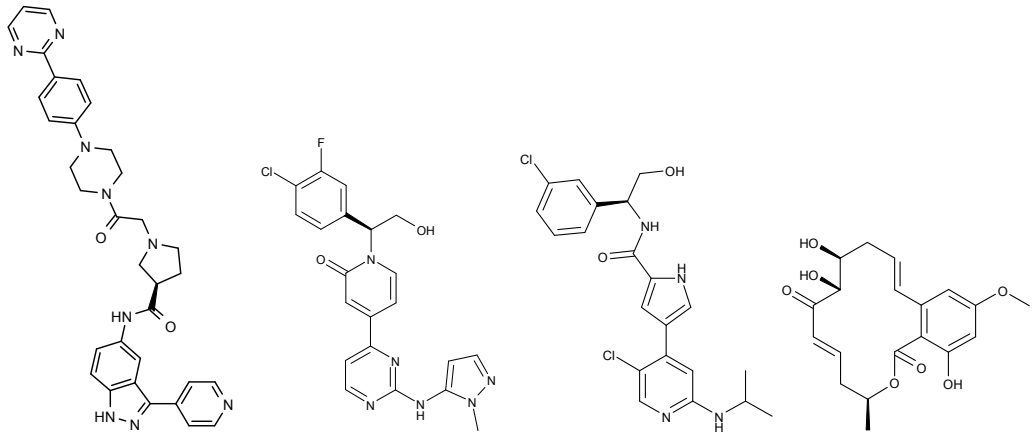

Figure 1 – Selection of published ERK1/2 inhibitors (Left to right, SCH772984, GDC-0994, BVD-523 and FR148083).

Covalent (irreversible and or reversible) inhibitors have a number of potential advantages over non-covalent small molecules which have been well documented and can include improved selectivity and increased activity (or prolonged duration of activity) against the primary target[23]. However, covalent inhibitors do have potential risks such as idiosyncratic toxicity, if they are susceptible to binding covalently to a range of targets. In addition, if an inhibitor acting with a short duration of action is preferred then an irreversible covalent inhibitor might not be suitable as the pharmacodynamic (PD) effect often continues after the compound has been metabolised and cleared from the body. With specific reference to ERK, a covalent inhibitor may have the advantage of maximum pathway knockdown along with a differential effect on feedback mechanisms to non-covalent inhibitors; however there is the potential for toxicity through total inhibition of this key signalling pathway which is also utilised by non-tumorigenic cells. Therefore the identification of potent and selective covalent inhibitors of ERK1/2, with suitable properties for in vitro and in vivo experiments, will enable the risks and benefits of such a profile to be further evaluated.

Results and discussion

Series Identification. Two hit identification approaches were taken to design and develop covalent inhibitors of ERK1/2. The first approach consisted of the direct modification of published ERK1/2 inhibitors, through addition of a covalent 'war-head' in a suitable position on the molecule informed by knowledge of the likely binding mode (along with location of Cys-166) through molecular modelling. As an alternative approach, we identified a set of non-covalent ERK1/2 inhibitor template from high throughput screening (HTS) to similarly convert to covalent inhibitors through molecular modelling and structurally informed addition of a covalent functionality.

Assessment of the binding mode of published ERK1/2 inhibitors via molecular modelling, suggested tetrahydro-pyrido-pyrimidine[18], indazole[24] and tetrahydro-pyrazolo-pyridine[25] scaffolds might be suitable starting points for this approach. Inhibitors containing these scaffolds were computationally docked into ERK2 crystal structures using Glide to model potential binding modes (PDB Code 2OJI[20]). The Cys-166 residue appears to be in a relatively challenging region of the ATP pocket to target. It is potentially incompatible in terms of the vectors associated with some hinge scaffolds and established (irreversible) covalent warheads. The impact of this is that there is a requirement for a specific geometry of suitable linker groups for the covalent warhead to be correctly positioned. A range of target compounds for possible synthesis were evaluated using covalent docking, where a variety of reactive groups were positioned on different regions of the described scaffolds. Molecular modelling studies indicated that a sulphonamide group might facilitate a suitable geometry to target Cys-166 from the highlighted scaffolds which were predicted to bind to the hinge region. Three target compounds were synthesised (**1**, **2** and **3**), for examples **1** and **2** additional compounds were made (**4** and **5**) without the double bond of the reactive group reduced as reversible control compounds (table 1).

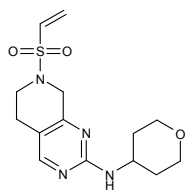

1

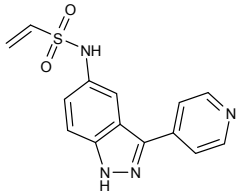

2

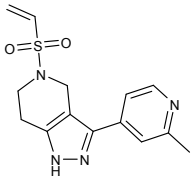

3

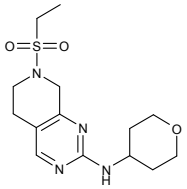

4

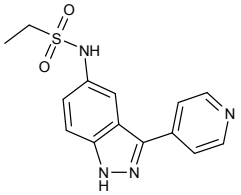

5

	BVD-523	**SCH772984**	**FR148083**	**1 (4)**	**2 (5)**	**3**
ERK2 Biochemical, K_M ATP (μM)	<0.0003	<0.0003	5.1	0.37 (9.0)	0.0075 (0.28)	0.074
ERK2 Biochemical, High ATP (μM)	<0.0003	<0.0003	3.7	0.22 (>10)	0.017 (1.8)	0.11
Cell MOA A375 pERK/pRSK (μM)	4.1/0.14	0.004/0.02	1.6/5.7	0.24/1.1 (10/>30)	0.12/0.47 (10/>30)	0.38/1
Cell Proliferation A375 (μM)	0.18	0.07	4.1	ND (ND)	1.3 (>30)	1.4
MEK1 Biochemical, K_M ATP (μM)	>10	>10	3.4	>10	>10	4.9
Log $D_{7.4}$[a]	>4	3.2	1.6	1	2.2	1.6
Aqueous Solubility (μM)[b]	8.5	<2.1	47	760	7	300
Kinase Selectivity	ND	ND	ND	2 (C-RAF,	8 (AURB,	5 (C-RAF,

(N>75% out of 125 Kinase panel)				**MEK1**)	AURC, c-RAF, **FLT1**, **FLT3**, **KDR**, MKK7b, TRKA)	**FLT1**, **KDR**, **MEK1**, PRAK)

Activity data into parenthesis indicates data on non-covalent matched pairs **4** and **5**. All IC_{50} data are reported as micromolar and are the mean of at least n=2 independent measurements. Kinase selectivity data measured at 1 μM compound concentration. Kinases in bold have a cysteine in the same position as Cys-166 in ERK2. ND is not determined. [a]Distribution coefficient between 1-octanol and aqueous phosphate buffer at pH 7.4. [b]Solubility of compounds in aqueous phosphate buffer at pH 7.4 after 24 hours at 25 °C (μM).

Table 1 – Covalent inhibitors exploiting published ERK1/2 inhibitor templates.

All three of the designed compounds (**1, 2** and **3**) showed promising ERK2 biochemical activity at K_M ATP (60 μM) and broadly equivalent activity using higher concentrations of ATP (1 mM). For these compounds we also observed promising cellular activity in a mechanism of action (MOA) assay measured by the levels of phosphorylated ERK2 (pERK) and of the phosphorylation of the downstream kinase RSK (pRSK) in an A375 melanoma cell line, containing a b-RAF^{V600E} mutation. In contrast, in our assays FR148083 showed only weak biochemical activity and weak cellular activity. Additionally, the enzyme-cell drop-off for disclosed inhibitors BVD-523 and SCH772984 is significantly greater (likely driven by competition with cellular ATP) compared to the covalent inhibitors, as expected with a covalent mechanism of action. The impact on the level of pErk suggests that these compounds are also preventing the activation of ERK2 kinase (in addition to the inhibition of catalysis); this shows a profile broadly similar to SCH772984 as opposed to BVD-523 which has a profile consistent with the inhibition of catalysis only. Anti-proliferative effects in this A375 melanoma cell line were also detected for these novel compounds, albeit weakly which may be due to high intrinsic compound reactivity, discussed later. In both cases where we synthesised comparative compounds without the reactive functionality (examples **4** and **5**), the compounds were significantly less active across these assays highlighting the importance of the covalent war-head to activity. The covalent binding mechanism of **1** and **2** was confirmed by Mass Spec (Supplementary Figures S1 and S2), there was not enough sample available to confirm this mechanism for **3**. The binding mode of **1** was resolved using co-crystallisation (Figure 2). As predicted by the modelling work, the inhibitor makes key hydrogen bonding interactions at the hinge region with residues Leu-107 and Met-108, both with hydrogen bond distances of 1.9Å. The sulphonamide group also makes an interaction with a bound water molecule, which forms an intricate network of hydrogen bonds to Gln-105, the backbone of Asp-167 and Lys-54. The covalent bond formed with Cys-166 was clearly observed in the electron density. Interesting, when compound **1** was soaked into ERK2 crystals, the inhibitor was unable to form a covalent bond with Cys-166 (data not shown). This may suggest that a degree of protein reorganisation is required for the covalent reaction to occur which was not possible when the compound was soaked into the crystal system. The docking calculation largely reproduced the crystallographic binding mode; the discussed bound water molecule however was not included in the simulation as all crystallographic water molecules were removed. However, the predicted direct interaction of sulphonamide group with Lys-54 appears to stabilise this interaction in the docking studies resulting in the crystallographic binding mode maintaining a favourable GlideScore.

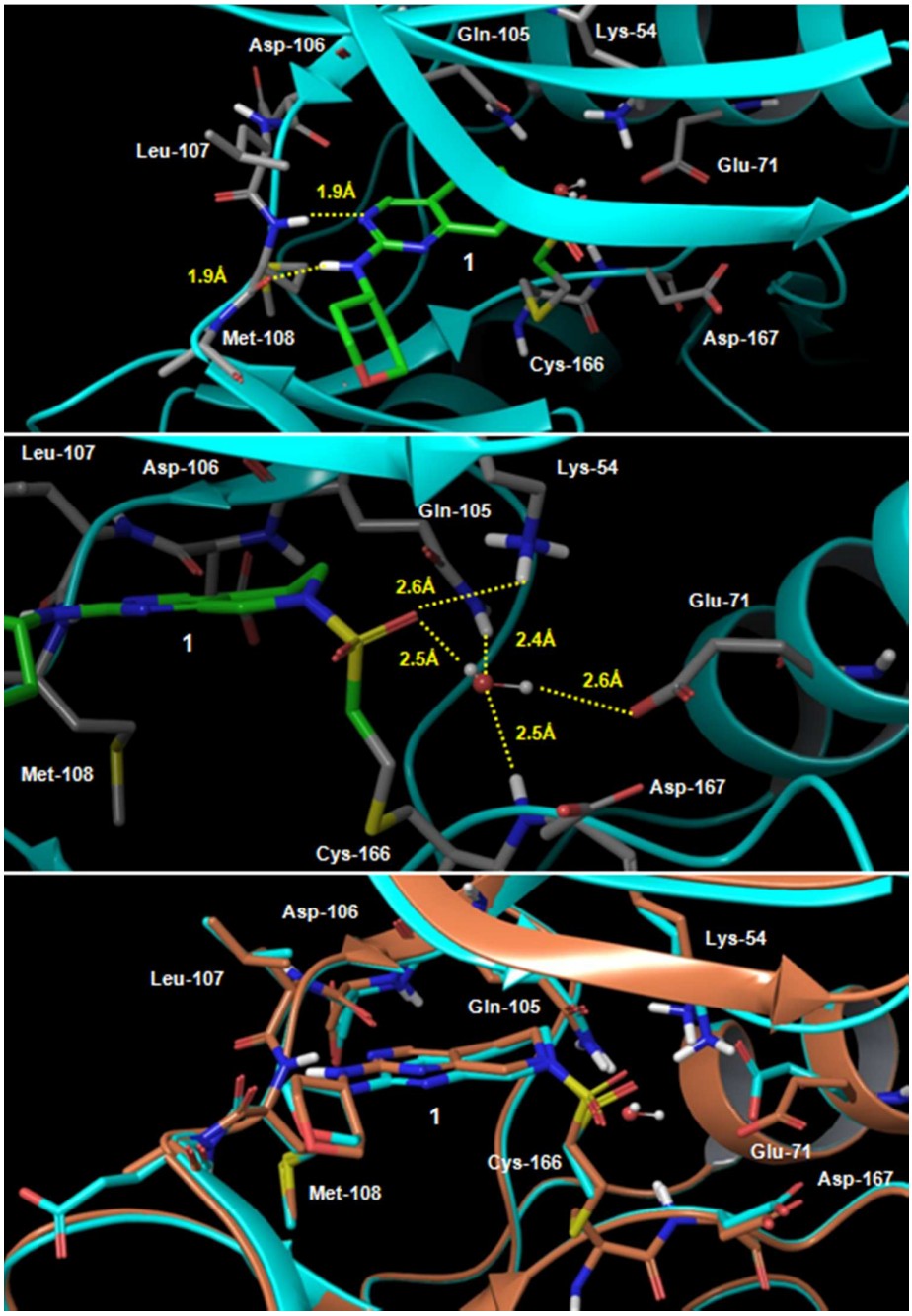

Figure 2 - Binding mode of compound **1** elucidated in human ERK2 crystal structure via co-crystallisation (PDB Code 4ZZM). Top figure highlights the interaction of the pyrimidine group with the hinge region. The middle figure shows the hydrogen bond network around the sulphonamide group and bound crystallographic water molecule. The lower figure shows the crystal structure in blue, compared to the docked pose in brown using the covalent docking protocol in Glide (Using PDB Code 2OJI).

The lipophilicity of these molecules (measured by LogD at pH 7.4) is relatively low which, along with their relatively small molecular size, suggests scope for further optimisation and the physicochemical properties such as solubility were also encouraging. Broader kinase selectivity was assessed through testing in a Eurofins (Millipore)[26] sub-panel of 125 kinases. Compound **1** in particular showed very good kinome selectivity which is perhaps surprising for compounds of such low

complexity, which make a relatively small number of interactions in the binding site. It was reassuring to confirm that these compounds did not appear to be active against all kinases with a cysteine in this region, as was reported with analogues of hypothemycin. It is important to note that the Eurofins (Millipore) assays for RAF and MEK1 are coupled assays, thereby compounds active in ERK1/2 may also appear active against RAF and MEK1. The MEK1 assay contains unactive ERK2, with the c-RAF assay containing unactive MEK1 and ERK2. Compounds **1** and **2** were subsequently confirmed as inactive (IC_{50} >10 μM) against an in-house MEK1 biochemical assay, with **3** showing weak MEK1 activity of 4.9 μM. Identifying which additional kinases these compounds may act upon via a covalent mechanism of action was also of interest (i.e. kinases with a cysteine in the same position as Cys-166). Importantly, compound **1** did not appear to have significant kinase inhibition against this subset of kinases. For compounds **2** and **3** activity was observed only against a limited number of kinases that included KDR, FLT1 and FLT4. Although these compounds gave us confidence that Cys-166 could be selectively targeted with small molecules, these inhibitors proved difficult to further optimise as the sulphonamide war-head has high intrinsic reactivity to thiols which we were not able to substantially temper through modification whilst also maintaining target activity. In an assay measuring compound reactivity versus glutathione as a model for the active site cysteine residue, compound **1** demonstrated a $t_{1/2}$ of 15.4 minutes, compared to our recent disclosure of our EGFR mutant-selective inhibitor AZD9291, which had $t_{1/2}$ of 121 minutes[27] (Note in pH 7.4 buffer alone compound **1** is stable to hydrolysis showing no reaction over 11 hrs at 37°C). This difference in reactivity is driven by the alkenyl sulphonamide versus acrylamide warhead change. However, based on modelling, the alkenyl sulphonamide warhead was judged to have the most suitable vector to target Cys-166. High relative reactivity could lead to issues in the optimisation of pharmacokinetic (PK) properties and may also be more likely to result in non-specific covalent binding to a wider range of targets and instability when tested across in vitro assays.

From in-house screening using an ERK2 biochemical assay, a reversible inhibitor (**6**), first synthesised within our internal FAK drug discovery program, was identified[28]. This compound showed moderate potency (0.044 μM and 0.34 μM in the K_m and high ATP ERK2 biochemical assays) and we believed it was a suitable lead compound to enable further optimisation through the addition of reversible and irreversible interactions. ERK1 activity was also confirmed for this compound (0.095 μM) using the Eurofins (Millipore) kinase panel. In a bid to improve ERK1/2 potency and broader kinase selectivity, the tetrahydropyran (THP) group, which was predicted to bind in the solvent channel of disclosed ERK inhibitors[18], was hybridised onto our identified hinge binding group. We also decided to assess the impact of replacement of the tri-fluoro methyl group with chlorine. The resulting compounds **7** and **8** showed improvements in general kinase selectivity (**4** other kinases with >75% inhibition compared to **10**) whilst potency remained largely unchanged (table 2).

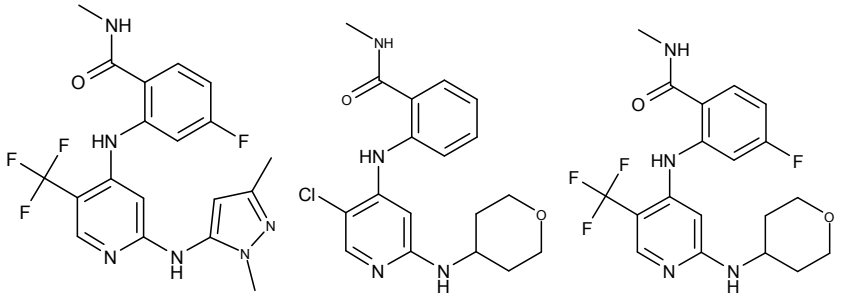

6 **7** **8**

	6	**7**	**8**
ERK2 Biochemical, K_M ATP (μM)	0.044	0.26	0.04
ERK2 Biochemical, High ATP (μM)	0.34	ND	0.38
Cell MOA A375 pERK/pRSK (μM)	8.7/5.1	7.5/10	2.1/2.4
Cell Proliferation A375 (μM)	1.4	ND	3.4
MEK1 Biochemical, K_M ATP (μM)	>10	>10	>10
Log $D_{7.4}$[a]	3.8	2.8	3.4
Aqueous Solubility (μM)[b]	15	290	8.8
Kinase Selectivity (N>75% out of 125 Kinase panel)	10 (AURB, AURC, AXL, CDK1, CDK7, c-RAF, IGF-1R, IR, MET, FAK, TRKA)	ND	4 (CDK7, c-RAF, MET, FAK)

Kinase selectivity data measured at 1 μM compound concentration. All IC_{50} data are reported as micromolar and are the mean of at least n=2 independent measurements. ND is not determined. [a]Distribution coefficient between 1-octanol and aqueous phosphate buffer at pH 7.4. [b]Solubility of compounds in aqueous phosphate buffer at pH 7.4 after 24 hours at 25 °C (μM).

Table 2 – Reversible ERK1/2 inhibitors identified from in-house screening.

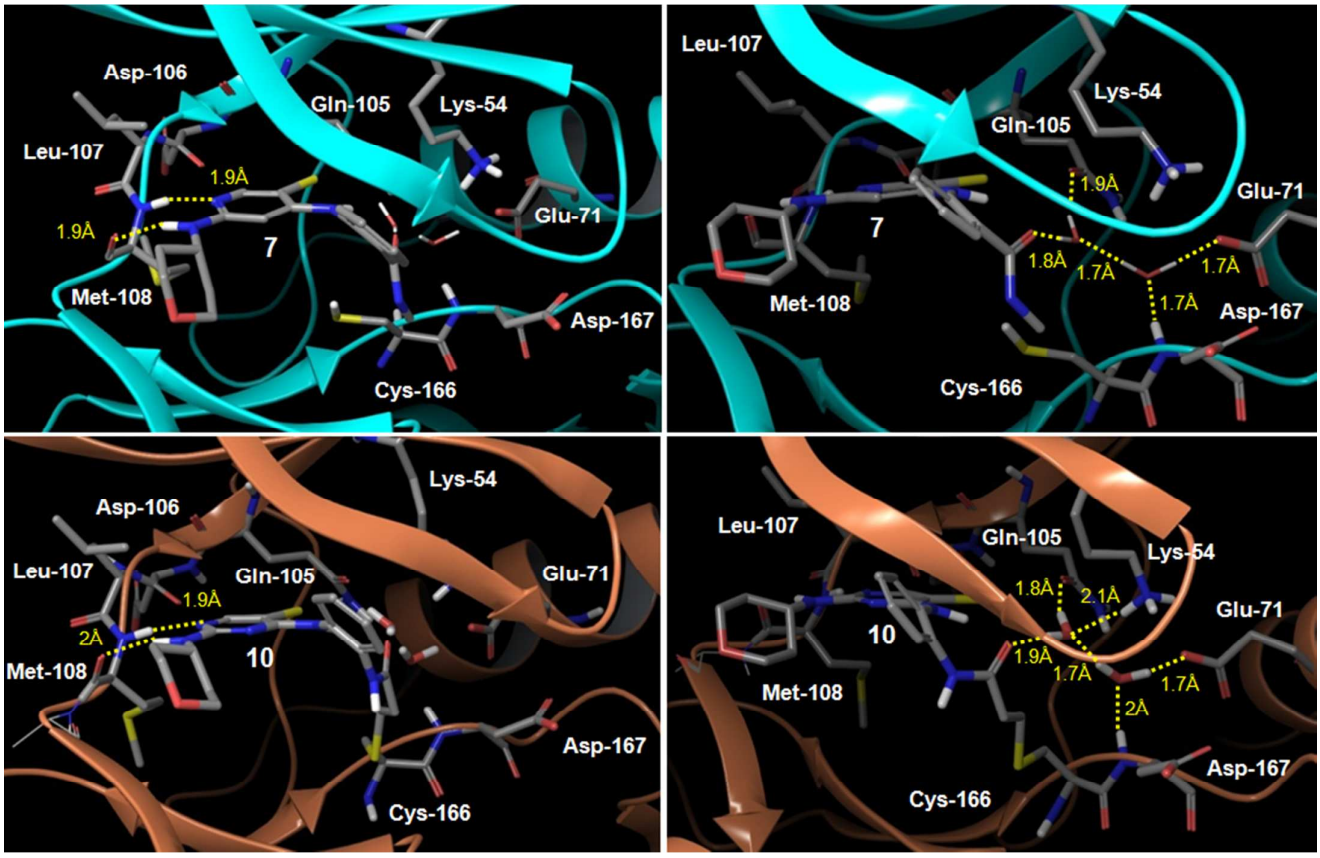

Figure 3 - Binding mode of **7** (blue) and **10** (brown) elucidated in human ERK2 crystal structure. Top figures show compound **7** (PDB Code 4ZZN), focusing on the hinge region interactions (left) and bound water molecules interactions (right). Lower figures show compound **10** (PDB Code 4ZZO), focusing on the hinge region interactions (left) and bound water molecules interactions (right).

To guide further development of this series, a crystal structure using compound soaking was solved for compound **7** (Figure 3). The crystal structure highlighted the important interaction of the pyridine group with the Met-108 located on the hinge region (two hydrogen bonds with lengths of 1.9Å). Also of particular interest were two identified crystallographic water molecules, one of which interacts directly with the amide of compound **7**, forming a network of hydrogen bonds with Glu-71, Gln-105 and Asp-167. The water molecule closest to the inhibitor was displaced by an oxygen of the sulphonamide of compound **1**. The positioning of this anilino group confirmed our hypothesis that substituting the aniline on the 2-position would be suitable to target Cys-166. A single compound was initially synthesised (**9**) which maintained the pyridine hinge binding group. Where the acrylamide functionality was located at the 2-position of the aniline, the amide was reversed to enable this chemical modification. This change appeared to be tolerated from the molecular modelling work as the key interactions appeared to be broadly maintained. The activity data on this first example was highly encouraging as good biochemical (0.042 μM K_m and 0.06 μM High ATP) and

cellular activity (0.12 μM pRSK and 0.4 μM pERK) were observed. Indeed, the potency increased when compared to the earlier covalent examples (Table 3). These compounds appeared to show effects on both pERK and pRSK, consistent with the activity profile of our earlier inhibitors and SCH772984. Subsequently, the matched pair with a pyrimidine hinge binding group was synthesised (**10**) to assess impact of this change on activity, the pyrimidine hinge region binding group having been observed in other ERK inhibitors such as GDC-0994. This demonstrated approximately 10-fold greater potency across our *in vitro* compound activity assays. It was also reassuring that these compounds showed reduced intrinsic reactivity towards glutathione compared to the earlier alkenyl sulphonamide series, with $t_{1/2}$ 152 minutes for **10**, suggesting a greater contribution of reversible interactions to overall compound potency for these compounds. The reversible matched pair of **10** (compound **11**) was also synthesised as a tool compound to assess the specific impact of the covalent bond, again showing significantly weaker activity across the assays. Mass Spectrometry was used to confirm covalent binding of **10** to ERK2, which as expected was not observed with **11** (Supplementary Figures S3 and S4). The binding mode of the covalent inhibitor **10** (brown) was solved using co-crystallisation and was remarkably similar to that of the reversible inhibitor **7** (Figure 3). It is interesting to note that even though the amide group has been reversed in compound **10** (compared to that of compound **7**), this apparently key interaction with the bound water molecule is largely maintained. This series of covalent inhibitors appears to be able to exploit this complex of water molecules to produce exquisite kinome selectivity; however compound **1** demonstrates that this selectivity can largely be maintained if these specific interactions can be replaced by the inhibitor. Both compounds **7** and **10** appear to have the binding mode stabilised by an internal hydrogen bond between the anilino NH and amide carbonyl, with a distance of 2Å in both cases. Compound **10** has consistent hydrogen bonding interactions with the hinge region residue Met-108 as **7** (distances of 1.9 Å and 2Å). One notable difference was the rotation of the Cys-166 side-chain which enables the formation of the covalent bond, highlighting some flexibility in the conformation of this residue.

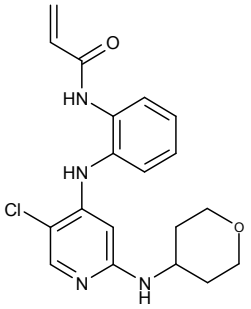

9

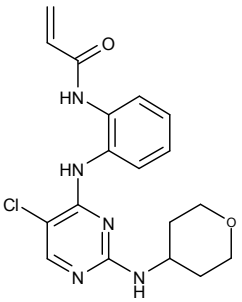

10

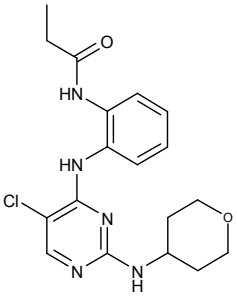

11

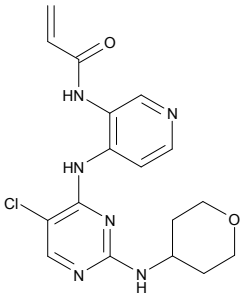

12

	9	**10(11)**	**12**
ERK2 Biochemical, K_M ATP (μM)	0.042	0.0085 (0.48)	0.0031
ERK2 Biochemical, High ATP (μM)	0.060	0.0054 (4.0)	0.003
Cell MOA A375	0.12/0.4	0.019/0.069 (>30/>30)	0.0067/0.028

pERK/pRSK (μM)			
Cell Proliferation A375 (μM)	0.68	0.057 (6.6)	0.041
MEK1 Biochemical, K_M ATP (μM)	>10	>10	>10
Log $D_{7.4}$[a]	2.5	2.7	2.3
Aqueous Solubility (μM)[b]	40	46	150
In-vitro Clearance HLM, (Rat Heps)[c]	24 (270)	67 (200)	13 (>250)
Kinase Selectivity (N>75% out of 125 Kinase panel)	2 (C-RAF, **MEK1**)	4 (AURB, AURC, c-RAF, **FLT1**)	2 (c-RAF, **MEK1**)

Activity data into parenthesis indicates data on non-covalent matched pair **11**. All IC_{50} data are reported as micromolar and are the mean of at least n=2 independent measurements. Kinase selectivity data measured at 1 μM compound concentration. Kinases in bold have a cysteine in the same position as Cys-166 in ERK2. [a]Distribution coefficient between 1-octanol and aqueous phosphate buffer at pH 7.4. [b]Solubility of compounds in aqueous phosphate buffer at pH 7.4 after 24 hours at 25 °C (μM). [c]Human microsome and rat hepatocytes metabolism intrinsic clearance (μL min^{-1} mg^{-1}).

Table 3 – Covalent ERK1/2 inhibitors developed from scaffold identified from in-house screening.

An additional compound (**12**) was synthesised in an effort to improve ERK1/2 potency through increasing the reactivity towards Cys-166, our previous studies indicated such a change is likely to increase the reactivity of the acrylamide towards glutathione[29]. This was the most potent compound synthesised within this early work and showed exquisite pan-kinase selectivity. As expected, the addition of the nitrogen increased the inherent reactivity of the acrylamide, with a $t_{1/2}$ 42 minutes in the glutathione assay (Both compounds **10** and **12** are stable to hydrolysis in pH 7.4 buffer alone at 37°C). Note as discussed previously, the compounds in this table were tested against our MEK1 biochemical assay, where they were inactive (IC_{50}>10μM) so it is likely compounds such as **12** are not genuinely active against any kinases in the Eurofins (Millipore) panel. Compound **12** was subsequently used as a highly selectivity and potent in-vitro tool for cellular wash-out experiments where the compound inhibited direct ERK substrate phosphorylation (p90RSK pThr359/Ser363) for up to 48 hours after the removal of compound (Figure 4a). This is broadly consistent with recent literature data reporting a half life of 54 hours for ERK2 protein in mouse fibroblasts, ERK1 protein with a half-life of 120 hours[30]. In addition, the cellular potency of compound **12** was measured in the pRSK cellular assay as a time-course, showing maximal potency of the compound between 20-30 hours (Figure 4b), which also appears consistent with these data.

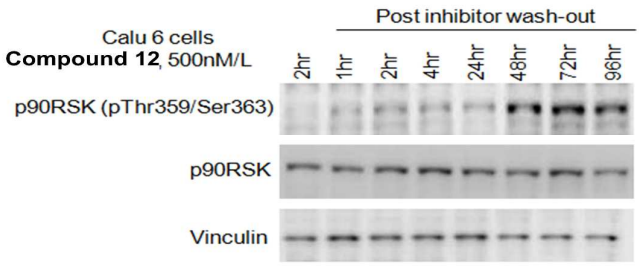

4a

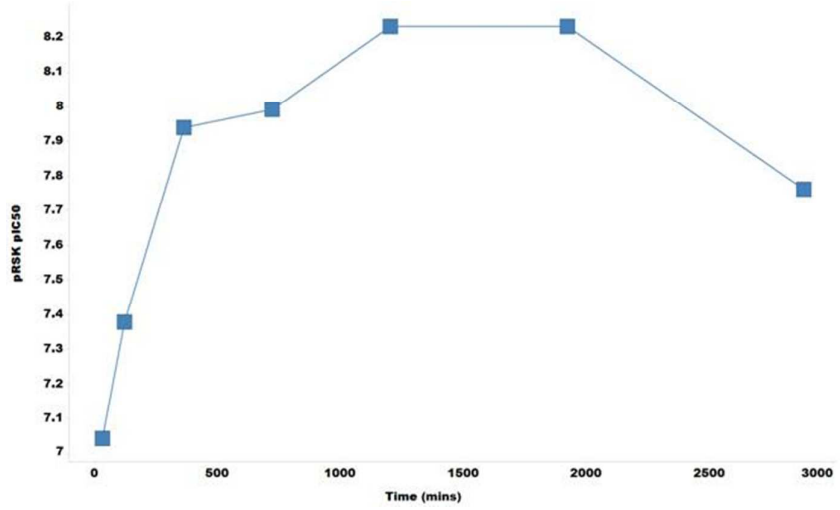

4b

Figure 4 – Cellular wash-out experiment with covalent ERK1/2 inhibitor **12** (4a) and pRSK cellular assay time-course study (4b).

Further development of the series was focused towards understanding the wider SAR around the template, with a particular target of identifying compounds which might be suitable for *in-vivo* testing. Our initial focus was to modify the 5-position of the pyrimidine along with the solvent channel group to vary the specific structural motifs and broader lipophilicity, with a view to impacting on compound plasma clearance. Due to the increased glutathione reactivity of compound **12**, we chose to revert back to the scaffold of **10**, where the acrylamide was attached to the phenyl group, to maximise our chances of improving pharmacokinetic properties.

Modification to the 5-position of the pyrimidine was tolerated with a number of groups. The CF_3 analogue was a particularly potent example (**13**), with methyl also showing activity (**14**, Table 4). We also observed that the THP group could be replaced by a pyrazole (**15**), or certain basic-containing motifs such as compound **16**. These changes were also combined in example **17**. The emerging data suggested that lowering $LogD_{7.4}$ of compounds in this series broadly resulted in decreased in-vitro metabolic clearance, correlations show an R^2 of 0.69 when log human microsome clearance is plotted against $LogD_{7.4}$ (Supplementary Figure S4). We were however concerned with compounds where $LogD_{7.4}$ has been significantly lowered as this might negatively impact on passive compound permeability into cells. Therefore our aim was to target an area of liopophilicity which gave a

suitable compromise between these properties. It was also observed that whilst compounds with the THP and basic functionality in the solvent channel tested as inactive in the MEK1 biochemical assay, examples with pyrazole did show increased activity (0.12μM for **15** and 0.26 uM for **17**). These data might suggest that it is possible to find a relatively selective, dual MEK1/ERK, covalent inhibitor through the approach described here.

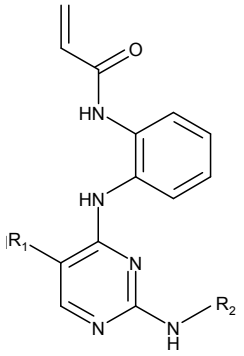

	13	**14**	**15**	**16**	**17**
R_1	CF_3	Me	Cl	Cl	Me
R_2				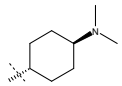	
ERK2 Biochemical, K_M ATP (μM)	0.0069	0.077	0.0099	0.085	0.039
ERK2 Biochemical, High ATP (μM)	0.0085	0.088	0.013	0.090	0.047
Cell MOA A375 pERK/pRSK (μM)	0.022/0.065	0.17/0.74	0.048/0.12	0.072/0.2	0.066/0.28
Cell Proliferation A375 (μM)	0.053	0.47	0.091	0.12	0.24
MEK1 Biochemical, K_M ATP (μM)	>10	>10	0.12	>10	0.26
Log $D_{7.4}$[a]	2.9	2	2.4	0.9	2.1
Aqueous Solubility (μM)[b]	59	170	520	770	990
In-vitro Clearance HLM, (Rat Heps)	38 (270)	13 (59)	42 (120)	<3 (25)	19 (33)
Kinase Selectivity (N>75% out of 125 Kinase panel)	6 (AURB, AURC, CDK7, c-RAF, **MEK1**, SRC)	2 (c-RAF, **MEK1**)	7 (AURB, AURC, c-RAF, **FLT1**, **KDR**, **MEK1**, FAK)	4 (c-RAF, DYRK2, **FLT1**, **MEK1**)	ND

Kinase selectivity data measured at 1 μM compound concentration. All IC_{50} data are reported as micromolar and are the mean of at least n=2 independent measurements. Kinases in bold have a cysteine in the same position as Cys-166 in ERK2. [a]Distribution coefficient between 1-octanol and aqueous phosphate buffer at pH 7.4. [b]Solubility of compounds in aqueous phosphate buffer at pH 7.4 after 24 hours at 25 °C (μM).

Table 4 – Expansion of SAR around the pyrimidine template

From this set of compounds, considering compound potency, broader kinase selectivity and physicochemical properties we identified compound **13** as a potential *in-vivo* tool compound for mouse studies. Although *in vivo* plasma clearance in mouse appeared high (note *in vitro* clearance in mouse hepatocytes was high, 143 μL/min/10^6 cells), when compound **13** was co-dosed with the irreversible inhibitor of cytochrome P450's, 1-aminobenzotriazole (ABT), we were able to estimate that the inhibitor could achieve 9 and 7-fold free plasma cover above cellular pRSK IC_{50} at the 0.5 and 2 hr time points (Mouse oral $AUC_{0\text{-}t}$ (μM.h) of 21) respectively which for an irreversible agent could be adequate to explore the *in vivo* pharmadynamic (PD) activity using established models in the mouse. In addition, the timecourse experiment shown in figure 4b suggests that the cellular potency of these inhibitors may increase over time, potentially giving increased levels or duration of cover than this calculation may suggest. As mouse or human plasma protein binding could not be measured due to poor recovery of compound, the fold-free cover was estimated using the protein binding value of the saturated analogue of compound **11** (Supplementary Figure S5).

Conclusion

We have described an approach for the identification of potent and selective irreversible covalent ERK1/2 inhibitors using the exploitation of published ERK inhibitors along with in-house biochemical screening. To our knowledge these are the first disclosed selective covalent ERK1/2 inhibitors fully characterised by biochemical and cellular assays along with elucidation of binding mode by x-ray crystallography[31]. Although our covalent inhibitors identified from published scaffold start points were active and showed good selectivity, a more potent and potentially developable series of compounds was identified through the optimisation of compounds identified from in-house screening. These compounds have excellent biochemical and cellular ERK potency and highlighted examples showed exquisite selectivity in broad kinase panels. The cellular activity of these compounds is equivalent to published inhibitors BVD-523 and SCH772984. However, they have reduced molecular weight and lower lipophilicity resulting in improved ligand efficiency (LE) and ligand lipophilicity efficiency (LLE)[32] along with an alternative mechanism of inhibition. We have also highlighted a compound which was dosed *in vivo* in mouse (with ABT) to give likely target coverage of at least 2 hours, thereby providing a potential *in vivo* tool compound for the pathway where the brief inhibition through a covalent mechanism of action may be adequate, or preferred. In summary, we have disclosed a series of highly potent and selective ERK1/2 inhibitors that will enable improved understanding of how to optimally inhibit the RAS/RAF/MEK/ERK signaling pathway.

Supporting Information Available: Additional data analyses, experimental information and compound characterisation can be found in the supporting information. This material is available free of charge via the Internet at http://pubs.acs.org.

Acknowledgements

We would like to thank all colleagues at AstraZeneca who were involved in the work reported in this manuscript.

Experimental

Chemistry

General Analytical Information

Nuclear Magnetic Resonance spectra were recorded on a Bruker 300 MHz, 400 MHz or 500 MHz instrument at room temperature. All ^{1}H NMR spectra were measured in part per million (ppm) relative to the signals for residual dimethyl sulfoxide (DMSO) in deuterated DMSO (2.52 ppm), or the signals for tetramethylsilane (TMS) added into the deuterated chloroform (0 ppm). Data for ^{1}H NMR were reported as: chemical shift, integration, multiplicity (s = singlet, d = doublet, t= triplet, q = quartet), coupling constants measures in Hz. Mass spectra were obtained on a Waters LCMS Micromass instrument with a XSELECT CSH™ C18, 5 μM, 2.1 x 50 mm column. All compounds were found to be of 95% purity or greater by LCMS.

Full compound synthesis experimental details and characterisation are detailed in the supplementary material with a selection of key examples shown below.

Representative procedure for the synthesis of vinyl sulfonamides 1, 2 and 3.

Scheme 1 - Synthesis of 4 – 3-(2-methylpyridin-4-yl)-5-(vinylsulfonyl)-4,5,6,7-tetrahydro-1 H-pyrazolo[4,3-c]pyridine **3.**

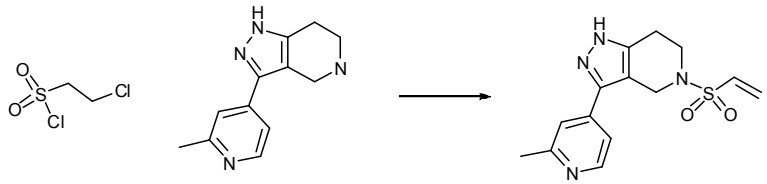

3a 3b 3

2-Chloroethanesulfonyl chloride (0.029 mL, 0.27 mmol) **3a** was added to 3-(2-methylpyridin-4-yl)-4,5,6,7-tetrahydro-1 H-pyrazolo[4,3-c]pyridine **3b** (58.8 mg, 0.27 mmol) and *N*-ethyl-*N*-isopropylpropan-2-amine (0.146 mL, 0.82 mmol) in DMF (2 mL). The resulting solution was stirred at room temperature for 24 hours. The solution was absorbed onto silica and purified by

flash silica chromatography, elution gradient 0 to 30% actetone in EtOAc. Pure fractions were evaporated to dryness to afford 3-(2-methylpyridin-4-yl)-5-(vinylsulfonyl)-4,5,6,7-tetrahydro-1 H-pyrazolo[4,3-c]pyridine **3** (33.0 mg, 39.5 %) as a colourless gum. ^{1}H NMR (400 MHz, DMSO) δ 2.57 (s, 3H), 2.88 (t, J = 5.7 Hz, 2H), 3.54 (t, J = 5.8 Hz, 2H), 4.52 (s, 2H), 6.16 (d, J = 10.0 Hz, 1H), 6.24 (d, J = 16.5 Hz, 1H), 6.95 (dd, J = 10.0, 16.5 Hz, 1H), 7.40 (d, J = 5.1 Hz, 1H), 7.49 (s, 1H), 8.54 (d, J = 5.2 Hz, 1H), 13.08 (s, 1H). HRMS: ESI$^+$ *m/z* calculated for $C_{14}H_{16}N_4O_2S$ $[M+H]^+$ 305.1072; *m/z* observed 305.1076.

Scheme 2 - Experimental procedures for the synthesis of *N*-(2-((5-chloro-2-((tetrahydro-2*H*-pyran-4-yl)amino)pyrimidin-4-yl)amino)phenyl)acrylamide **10.**

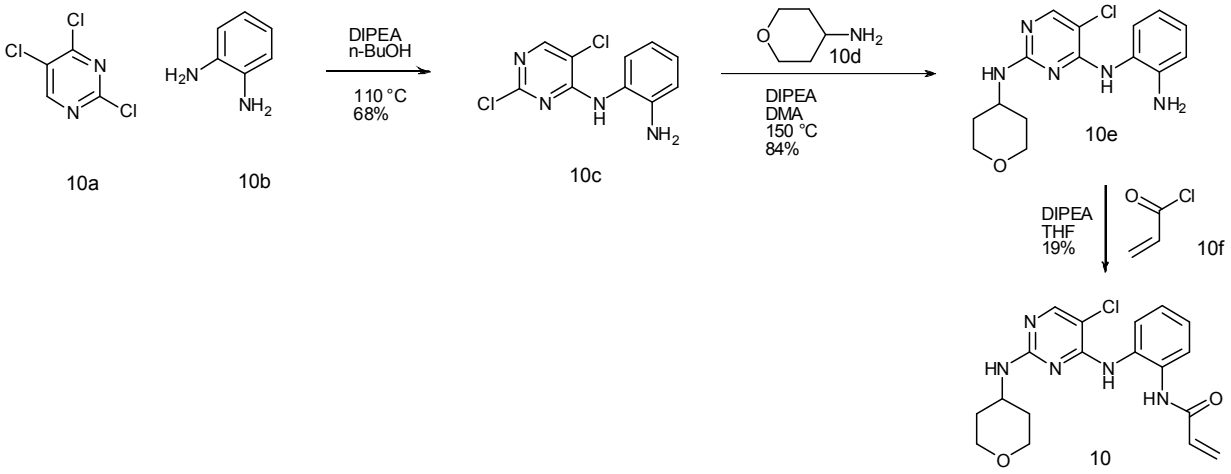

N-Ethyl-*N*-isopropylpropan-2-amine (1.90 mL, 10.9 mmol) was added to 2,4,5-trichloropyrimidine **10a** (1.00 g, 5.45 mmol) and benzene-1,2-diamine **10b** (0.590 g, 5.45 mmol) in n-butanol (25 mL) under nitrogen. The resulting solution was stirred at 110 °C for 3 hours. The reaction mixture was evaporated and the residue was stirred with aqueous HCl (0.1M, 10 mL) for 30 minutes. The solid was collected by filtration and dried under vacuum. The crude solid was triturated with DCM to give a solid which was collected by filtration and dried under vacuum to afford *N*1-(2,5-dichloropyrimidin-4-yl)benzene-1,2-diamine **10c** (0.942 g, 68%) as a white solid. Tetrahydro-2 H-pyran-4-amine **10d** (0.791 mL, 7.64 mmol), *N*1-(2,5-dichloropyrimidin-4-yl)benzene-1,2-diamine **10c** (650 mg, 2.55 mmol) and *N*-ethyl-*N*-isopropylpropan-2-amine (1.331 mL, 7.64 mmol) were dissolved in DMA (10 mL) and sealed into a microwave tube. The reaction was heated to 150 °C for 1 hour in the microwave reactor and cooled to 22 °C then evaporated to dryness. The residue was diluted with EtOAc (50 mL), and washed sequentially with water (50 mL) and saturated brine (50 mL). The organic layer was dried over $MgSO_4$, filtered and evaporated to afford crude product. The crude product was purified by flash silica chromatography, elution gradient 0 to 5% MeOH in DCM. Pure fractions were evaporated to dryness to afford *N*4-(2-aminophenyl)-5-chloro-*N*2-(tetrahydro-2 H-pyran-4-yl)pyrimidine-2,4-diamine **10e** (684 mg, 84%) as a white solid. A solution of acryloyl chloride **10f** (0.055 g, 0.611 mmol) in THF (3 mL) was added to a solution of *N*4-(2-

aminophenyl)-5-chloro-*N*2-(tetrahydro-2 H-pyran-4-yl)pyrimidine-2,4-diamine **10e** (0.195 g, 0.611 mmol) and *N*-ethyl-*N*-isopropylpropan-2-amine (0.156 mL, 0.910 mmol) in THF (10 mL) at 0 °C. The resulting solution was stirred at 0 °C under a nitrogen atmosphere for 35 minutes, then evaporated to dryness to afford a brown solid. The crude product was purified by silica gel chromatography, eluting with 25% to 75% ethyl acetate in heptane. Fractions containing pure product were combined and evaporated to dryness to afford *N*-(2-((5-chloro-2-((tetrahydro-2 H-pyran-4-yl)amino)pyrimidin-4-yl)amino)phenyl)acrylamide **10** (0.042 g, 19%). ^{1}H NMR (400 MHz, DMSO) □ 1.39 – 1.54 (m, 2H), 1.71 – 1.82 (m, 2H), 3.23 – 3.40 (m, 3H), 3.86 (d, *J* = 10.3 Hz, 2H), 5.85 (dd, *J* = 1.9, 10.1 Hz, 1H), 6.36 (dd, *J* = 1.8, 17.0 Hz, 1H), 6.55 (dd, *J* = 10.1, 17.0 Hz, 1H), 6.94 (s, 1H), 7.27 (dtd, *J* = 1.5, 7.5, 26.4 Hz, 2H), 7.43 (dd, *J* = 1.4, 7.8 Hz, 1H), 7.84 (d, *J* = 7.7 Hz, 1H), 7.99 (s, 1H), 8.33 (s, 1H), 10.20 (s, 1H). HRMS: ESI$^+$ *m/z* calculated for $C_{18}H_{20}ClN_5O_2$ $[M+H]^+$ 374. 1384; *m/z* observed 374.1398.

The non-covalent matched pair examples **4**, **5** and **11** were synthesised using the same methodology with the variation at the final step. The non-covalent inhibitors **7** and **8** were prepared in analogous way to 6[28], starting from the appropriate commercially available 2-chloropyridine.

Biochemical and Cellular Assays

A full description of compound handling and experimental methods for all biochemical and cellular assays referred to can be found in the supporting information section.

Molecular Modelling

The published ERK2 structure (pdb code 2OJI[20]) and in-house 4ZZN structures were used for the modelling of potential inhibitor binding modes from the fragment and HTS-derived work respectively. All crystallographic water molecules were deleted for the calculations as it was not deemed possible to confidently predict important water molecules upfront across the different series modelled. However, to validate this protocol, a series of docking calculations were performed to show the crystallographic inhibitors could be reliably re-docked into the protein structures with and without the water molecules highlighted in the manuscript. Crystal structures were prepared for docking using the protein preparation wizard in Maestro (Version 9.1, Schrodinger), which optimises hydrogen placements. The active site was defined by the bound ligand. Glide was used for the protein-ligand docking, in XP protocol. Multiple tautomers and protonation states were enumerated for ligands using our in-house software Leatherface[33]. A 3D structure of each ligand as input to the docking calculation was initially generated by Corina and optimised with the MMFF force field (Sheffield solvation model[34]). Docked binding modes were ranked using the docking score (GlideScore[35]) and visually inspected for the retention of key interactions to the hinge region (Leu-107) along with other

close contacts. Binding modes were deprioritised if the conformation of the docked molecule was considered unsatisfactory. The covalent docking algorithm in Glide was also used to assist the prioritisation of structures to covalently target Cys-166.

Mass Spectrometry and protein structures

Protein was incubated with compound present at 3 times the molar concentration of the ERK2 protein. After incubation at room temp for 2 hours, a small amount was diluted 10 fold for loading onto mass spectrometer immediately. Denaturing mass spec was performed by loading samples into Waters Premier QTOF via Agilent LC in solvents containing 0.05% formic acid. Each run lasted 5 minutes and was a single reverse phase binding step, which was followed by elution into the mass spectrometer in 90% acetonitrile to desalt sample. The remaining sample was used to set up crystallisation drops. Protein was set-up 1:1 with 30% polyethylene glycol monomethyl ether 2000, 200mM ammonium sulphate and 100 mM Hepes pH 7.6. Crystals appeared within a week. They were flash frozen in the presence of 15% v/v 2,3-butandiol and x-ray data collected at Dimond Light Source, (Didcot, UK).

6His-TEV-HsERK2(1-360)-LE

1 MHHHHHHGGG ENLYFQGSHM AAAAAAGAGP EMVRGQVFDV GPRYTNLSYI

51 GEGAYGMVCS AYDNVNKVRV AIKKISPFEH QTYCQRTLRE IKILLRFRHE

101 NIIGINDIIR APTIEQMKDV YIVQDLMETD LYKLLKTQHL SNDHICYFLY

151 QILRGLKYIH SANVLHRDLK PSNLLLNTTC DLKICDFGLA RVADPDHDHT

201 GFLTEYVATR WYRAPEIMLN SKGYTKSIDI WSVGCILAEM LSNRPIFPGK

251 HYLDQLNHIL GILGSPSQED LNCIINLKAR NYLLSLPHKN KVPWNRLFPN

301 ADSKALDLLD KMLTFNPHKR IEVEQALAHP YLEQYYDPSD EPIAEAPFKF

351 DMELDDLPKE KLKELIFEET ARFQPGYRSL E

Expected mw: 43829.8

Data collections were carried out at the Diamond Light Source synchrotron beamlines at cryogenic temperatures, using ethylene glycol as cryoprotectant. The pipedream and autoBUSTER software packages were used to solve and refine the structures, the program Coot was used for manual building of the models. Data collection and refinement statistics together with PDB accession codes of the final models are listed below. The structures have been deposited in the pdb as 4ZZM, 4ZZN and 4ZZO (Table 5).

Compound	1	7	10
PDB accession code	4ZZM	4ZZN	4ZZO
Data collection statistics			
Space group and cell par:	$P2_1$	$P2_1$	$P2_1$

a, b,c [Å] β [°]	48.88, 70.31, 60.41 109.12	48.76, 69.70, 59.80 108.71	48.75, 70.07, 60.10 109.25
Resolution [Å]	1.89	1.50	1.63
Unique reflections	30202 (2182)	55281 (1580)	47270 (3474)
Multiplicity	3.2 (3.2)	3.1 (2.2)	3.3 (3.2)
Completeness [%]	97.5 (94.1)	91.1 (53.1)	99.3 (98.8)
R_{sym} [%]	8.6 (57.3)	2.9 (9.3)	7.2 (56.7)
Mean(I)/sd	8.9 (1.9)	22.4 (6.3)	9.9 (2.1)
Refinement statistics			
Number of reflections (working /test)	30183 (1903)	61548 (2460)	47250 (2593)
R/R_{free} [%]	21.04/25.44	17.47/20.23	19.13/23.73
Deviation from ideal geometry bond lengths [Å] bond angles [◦]	 0.010 0.990	 0.012 1.060	 0.010 1.010
Ramachandran plot [%] preferred region generously allowed region disallowed region	 95.6 3.5 0.8	 96.71 2.4 0.9	 96.1 2.9 0.9

[‡] Data in parentheses refer to the highest resolution shell.

Table 5 – Protein crystal structure statistics.

Immunoblotting

Cells were washed on ice with cold PBS before the addition lysis buffer containing 25mmol/L Tris-HCl, 3 mmol/L EDTA, 3 mmol/L EGTA, 50 mmol/L sodium fluoride, 2 mmol/L sodium orthovanadate, 10mmol/L β-glycerophosphate, 5mmol/L pyrophosphate, 0.5% Triton X-100, 0.1% β-mercaptoethanol supplemented with protease inhibitor cocktail (Roche). After scraping, lysates were transferred to microcentrifuge tubes and shaken at 4°C for 20 minutes before 10-minute centrifugation and protein quantification with Bradford Reagent (Bio-Rad). Equal protein amounts were loaded for SDS-PAGE using 4-20% Tris-HCl gels (Bio-Rad) followed by transfer to nitrocellulose membranes. After blocking in 5% BSA-TBST or milk-TBST,

membranes were blotted with total p90RSK (BD Bioscience 610226), phospho-p90RSK (Thr359/Ser363, Cell Signaling Technology 9344) and vinculin (Sigma V9131) followed by horseradish peroxidase (HRP)–conjugated secondary antibodies (Cell Signaling Technology; 7074 or 7076). Signals were detected with SuperSignal West Dura Chemiluminescent Substrate, Thermo Scientific.

References

1. Schirmer, A.; Kennedy, J.; Murli, S.; Reid, R.; Santi, D. V. Targeted covalent inactivation of protein kinases by resorcylic acid lactone polyketides. *Proc. Natl. Acad. Sci. U. S. A.* 2006, *103,* 4234-4239.

2. Dhillon, A. S.; Hagan, S.; Rath, O.; Kolch, W. MAP kinase signalling pathways in cancer. *Oncogene* 2007, *26,* 3279-3290.

3. Hanahan, D.; Weinberg, R. A. The hallmarks of cancer. *Cell* 2000, *100,* 57-70.

4. Yoon, S.; Seger, R. The extracellular signal-regulated kinase: multiple substrates regulate diverse cellular functions. *Growth Factors* 2006, *24,* 21-44.

5. Owens, D. M.; Keyse, S. M. Differential regulation of MAP kinase signalling by dual-specificity protein phosphatases. *Oncogene* 2007, *26,* 3203-3213.

6. Vakiani, E.; Solit, D. B. KRAS and BRAF: drug targets and predictive biomarkers. *J. Pathol.* 2011, *223,* 219-229.

7. Solit, D. B.; Garraway, L. A.; Pratilas, C. A.; Sawai, A.; Getz, G.; Basso, A.; Ye, Q.; Lobo, J. M.; She, Y.; Osman, I.; Golub, T. R.; Sebolt-Leopold, J.; Sellers, W. R.; Rosen, N. BRAF mutation predicts sensitivity to MEK inhibition. *Nature* 2006, *439,* 358-362.

8. Ji, Z.; Flaherty, K. T.; Tsao, H. Targeting the RAS pathway in melanoma. *Trends Mol. Med.* 2012, *18,* 27-35.

9. Flaherty, K. T.; Infante, J. R.; Daud, A.; Gonzalez, R.; Kefford, R. F.; Sosman, J.; Hamid, O.; Schuchter, L.; Cebon, J.; Ibrahim, N.; Kudchadkar, R.; Burris, H. A.,3rd; Falchook, G.; Algazi, A.; Lewis, K.; Long, G. V.; Puzanov, I.; Lebowitz, P.; Singh, A.; Little, S.; Sun, P.; Allred, A.; Ouellet, D.; Kim, K. B.; Patel, K.; Weber, J. Combined BRAF and MEK inhibition in melanoma with BRAF V600 mutations. *N. Engl. J. Med.* 2012, *367,* 1694-1703.

10. Montagut, C.; Sharma, S. V.; Shioda, T.; McDermott, U.; Ulman, M.; Ulkus, L. E.; Dias-Santagata, D.; Stubbs, H.; Lee, D. Y.; Singh, A.; Drew, L.; Haber, D. A.; Settleman, J. Elevated CRAF as a potential mechanism of acquired resistance to BRAF inhibition in melanoma. *Cancer Res.* 2008, *68,* 4853-4861.

11. Wagle, N.; Emery, C.; Berger, M. F.; Davis, M. J.; Sawyer, A.; Pochanard, P.; Kehoe, S. M.; Johannessen, C. M.; Macconaill, L. E.; Hahn, W. C.; Meyerson, M.; Garraway, L. A. Dissecting therapeutic resistance to RAF inhibition in melanoma by tumor genomic profiling. *J. Clin. Oncol.* 2011, *29,* 3085-3096.

12. Emery, C. M.; Vijayendran, K. G.; Zipser, M. C.; Sawyer, A. M.; Niu, L.; Kim, J. J.; Hatton, C.; Chopra, R.; Oberholzer, P. A.; Karpova, M. B.; MacConaill, L. E.; Zhang, J.; Gray, N. S.; Sellers, W. R.; Dummer, R.; Garraway, L. A. MEK1 mutations confer resistance to MEK and B-RAF inhibition. *Proc. Natl. Acad. Sci. U. S. A.* 2009, *106,* 20411-20416.

13. Poulikakos, P. I.; Persaud, Y.; Janakiraman, M.; Kong, X.; Ng, C.; Moriceau, G.; Shi, H.; Atefi, M.; Titz, B.; Gabay, M. T.; Salton, M.; Dahlman, K. B.; Tadi, M.; Wargo, J. A.; Flaherty, K. T.; Kelley, M. C.; Misteli, T.; Chapman, P. B.; Sosman, J. A.; Graeber, T. G.; Ribas, A.; Lo, R. S.; Rosen, N.; Solit, D. B. RAF inhibitor resistance is mediated by dimerization of aberrantly spliced BRAF(V600E). *Nature* 2011, *480,* 387-390.

14. Morris, E. J.; Jha, S.; Restaino, C. R.; Dayananth, P.; Zhu, H.; Cooper, A.; Carr, D.; Deng, Y.; Jin, W.; Black, S.; Long, B.; Liu, J.; Dinunzio, E.; Windsor, W.; Zhang, R.; Zhao, S.; Angagaw, M. H.; Pinheiro, E. M.; Desai, J.; Xiao, L.; Shipps, G.; Hruza, A.; Wang, J.; Kelly, J.; Paliwal, S.; Gao, X.; Babu, B. S.; Zhu, L.; Daublain, P.; Zhang, L.; Lutterbach, B. A.; Pelletier, M. R.; Philippar, U.; Siliphaivanh, P.; Witter, D.; Kirschmeier, P.; Bishop, W. R.; Hicklin, D.; Gilliland, D. G.; Jayaraman, L.; Zawel, L.; Fawell, S.; Samatar, A. A. Discovery of a novel ERK inhibitor with activity in models of acquired resistance to BRAF and MEK inhibitors. *Cancer. Discov.* 2013, *3,* 742-750.

15. BVD-523. BioMed Valley Discoveries. https://biomed-valley.com/portfolio/bvd-523, *Accessed April 2015.*

16. GDC-0994. Proceedings: AACR Annual Meeting 2014; April 5-9, 2014; San Diego, CA. Robarge, K et al. Genentech, Inc., South San Francisco, CA; Array Biopharma, Boulder, CO.

17. Deng, Y.; Shipps, G. W.,Jr; Cooper, A.; English, J. M.; Annis, D. A.; Carr, D.; Nan, Y.; Wang, T.; Zhu, H. Y.; Chuang, C. C.; Dayananth, P.; Hruza, A. W.; Xiao, L.; Jin, W.; Kirschmeier, P.; Windsor, W. T.; Samatar, A. A. Discovery of novel, dual mechanism ERK inhibitors by affinity selection screening of an inactive kinase. *J. Med. Chem.* 2014, *57,* 8817-8826.

18. Blake, J. F.; Gaudino, J. J.; De Meese, J.; Mohr, P.; Chicarelli, M.; Tian, H.; Garrey, R.; Thomas, A.; Siedem, C. S.; Welch, M. B.; Kolakowski, G.; Kaus, R.; Burkard, M.; Martinson, M.; Chen, H.; Dean, B.; Dudley, D. A.; Gould, S. E.; Pacheco, P.; Shahidi-Latham, S.; Wang, W.; West, K.; Yin, J.; Moffat, J.; Schwarz, J. B. Discovery of 5,6,7,8-tetrahydropyrido[3,4-d]pyrimidine inhibitors of Erk2. *Bioorg. Med. Chem. Lett.* 2014, *24,* 2635-2639.

19. Aronov, A. M.; Tang, Q.; Martinez-Botella, G.; Bemis, G. W.; Cao, J.; Chen, G.; Ewing, N. P.; Ford, P. J.; Germann, U. A.; Green, J.; Hale, M. R.; Jacobs, M.; Janetka, J. W.; Maltais, F.; Markland, W.; Namchuk, M. N.; Nanthakumar, S.; Poondru, S.;

Straub, J.; ter Haar, E.; Xie, X. Structure-guided design of potent and selective pyrimidylpyrrole inhibitors of extracellular signal-regulated kinase (ERK) using conformational control. *J. Med. Chem.* 2009, *52,* 6362-6368.

20. Aronov, A. M.; Baker, C.; Bemis, G. W.; Cao, J.; Chen, G.; Ford, P. J.; Germann, U. A.; Green, J.; Hale, M. R.; Jacobs, M.; Janetka, J. W.; Maltais, F.; Martinez-Botella, G.; Namchuk, M. N.; Straub, J.; Tang, Q.; Xie, X. Flipped out: structure-guided design of selective pyrazolylpyrrole ERK inhibitors. *J. Med. Chem.* 2007, *50,* 1280-1287.

21. Ohori, M.; Kinoshita, T.; Yoshimura, S.; Warizaya, M.; Nakajima, H.; Miyake, H. Role of a cysteine residue in the active site of ERK and the MAPKK family. *Biochem. Biophys. Res. Commun.* 2007, *353,* 633-637.

22. Leproult, E.; Barluenga, S.; Moras, D.; Wurtz, J. M.; Winssinger, N. Cysteine mapping in conformationally distinct kinase nucleotide binding sites: application to the design of selective covalent inhibitors. *J. Med. Chem.* 2011, *54,* 1347-1355.

23. Singh, J.; Petter, R. C.; Baillie, T. A.; Whitty, A. The resurgence of covalent drugs. *Nat. Rev. Drug Discovery* 2011, *10,* 307-317.

24. Cooper, A.; Deng, Y.; Shipps Jr., G. W; Shih, N-Y.; Zhu, H.; Sun, R.; Kelly, .J; Doll, R.; Nan, Y.; Wang, T.; Desai, J.; Wang, J.; Dong, Y.; Madison, V. S.; Li, X.; Hruza, A.; Siddiqui, M. A.; Samatar, A.; Paliwal, S.; Tsui, H-C.; Celebi, A. A.; Wu, Y.; Boga, S. B. WO2007070398, Schering Corporation; 2000 Galloping Hill Road, Kenilworth, NJ 07033-0530, US.

25. Cooper, A.; Deng, Y.; Shipps Jr., G. W.; Sun, B.; Wang, J.; Zhu, L. WO2012036997, Schering Corporation; 2000 Galloping Hill Road, Kenilworth, NJ 07033-0530, US.

26. Eurofins (Millipore), http://www.eurofins.co.uk, *Accessed April 2015.*

27. Finlay, M. R.; Anderton, M.; Ashton, S.; Ballard, P.; Bethel, P. A.; Box, M. R.; Bradbury, R. H.; Brown, S. J.; Butterworth, S.; Campbell, A.; Chorley, C.; Colclough, N.; Cross, D. A.; Currie, G. S.; Grist, M.; Hassall, L.; Hill, G. B.; James, D.; James, M.; Kemmitt, P.; Klinowska, T.; Lamont, G.; Lamont, S. G.; Martin, N.; McFarland, H. L.; Mellor, M. J.; Orme, J. P.; Perkins, D.; Perkins, P.; Richmond, G.; Smith, P.; Ward, R. A.; Waring, M. J.; Whittaker, D.; Wells, S.; Wrigley, G. L. Discovery of a potent and selective EGFR inhibitor (AZD9291) of both sensitizing and T790M resistance mutations that spares the wild type form of the receptor. *J. Med. Chem.* 2014, *57,* 8249-8267.

28. Barlaam, B. C; Foote, K. M; Ple, P. WO2009153589, AstraZeneca UK Ltd; 15 Stanhope Gate London Greater London W1K 1LN, UK.

29. Ward, R. A.; Anderton, M. J.; Ashton, S.; Bethel, P. A.; Box, M.; Butterworth, S.; Colclough, N.; Chorley, C. G.; Chuaqui, C.; Cross, D. A.; Dakin, L. A.; Debreczeni, J. E.; Eberlein, C.; Finlay, M. R.; Hill, G. B.; Grist, M.; Klinowska, T. C.; Lane, C.; Martin, S.; Orme, J. P.; Smith, P.; Wang, F.; Waring, M. J. Structure- and reactivity-based development of covalent inhibitors of the activating and gatekeeper mutant forms of the epidermal growth factor receptor (EGFR). *J. Med. Chem.* 2013, *56,* 7025-7048.

30. Schwanhaeusser, B.; Busse, D.; Li, N.; Dittmar, G.; Schuchhardt, J.; Wolf, J.; Chen, W.; Selbach, M. Global quantification of mammalian gene expression control [Erratum to document cited in CA155:060687]. *Nature (London, U. K.)* 2013, *495,* 126-127.

31. Compounds sharing the pyrimidine scaffold have recently been disclosed as covalent inhibitors of Erk in a patent from Celgene Avilomics Research, Inc. Haq, N; Niu, D; Petter, R. C; Qiao, L; Singh, J; Zhu, Z. WO2014124230, Celgene Avilomics Research, Inc.

32. Hopkins, A. L.; Groom, C. R.; Alex, A. Ligand efficiency: a useful metric for lead selection. *Drug Discov Today* 2004, *9,* 430-431.

33. Lyne, P. D.; Kenny, P. W.; Cosgrove, D. A.; Deng, C.; Zabludoff, S.; Wendoloski, J. J.; Ashwell, S. Identification of Compounds with Nanomolar Binding Affinity for Checkpoint Kinase-1 Using Knowledge-Based Virtual Screening. *J. Med. Chem.* 2004, *47,* 1962-1968.

34. Grant, J. A.; Pickup, B. T.; Sykes, M. J.; Kitchen, C. A.; Nicholls, A. A simple formula for dielectric polarisation energies: The Sheffield Solvation Model. *Chem. Phys. Lett.* 2007, *441,* 163-166.

35. Friesner, R. A.; Murphy, R. B.; Repasky, M. P.; Frye, L. L.; Greenwood, J. R.; Halgren, T. A.; Sanschagrin, P. C.; Mainz, D. T. Extra Precision Glide: Docking and Scoring Incorporating a Model of Hydrophobic Enclosure for Protein-Ligand Complexes. *J. Med. Chem.* 2006, *49,* 6177-6196.

Table of Contents graphic

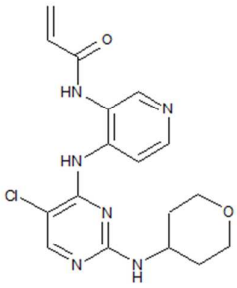

Erk2 Cell MOA (pRSK) = 0.028 μM